J. Water Environ. Nanotechnol., 7(2): 143-154 Spring 2022

ORIGINAL RESEARCH PAPER

Synthesis of Co and Cu codoped ZnO nanoparticles by citrate gel combustion method: Photocatalytic and antimicrobial activity

M. Sheik Muhideen Badhusha[1], B. Kavitha[2], M. Rajarajan[3*], P. Tharmaraj[4**], A. Suganthi[4]

[1] Department of Chemistry, Sadakathullah Appa College, Tirunelveli, India
[2] P.G. and Research Department of Chemistry, C.P.A. College, Bodinayakanur, India
[3] Directorate of Distance Education, Madurai Kamaraj University, Madurai- 625 021, India
[4] P.G. and Research Department of Chemistry, Thaiyaharajar College, Madurai, India

Received: 2022-02-10 Accepted: 2022-04-10 Published: 2022-05-01

ABSTRACT

ZnO, single-doped (Co-ZnO, Cu-ZnO), and co-doped ZnO ((Co, Cu)/ZnO) were effectively synthesized by the citrate gel combustion technique. The samples were characterized by UV-visible diffuse reflectance spectroscopy (UV-vis-DRS), Fourier transforms infrared spectroscopy (FT-IR), X-ray powder diffraction (XRD), Scanning electron microscopy (SEM), energy-dispersive X-ray spectroscopy (EDX) and photoluminescence spectroscopy (PL). The average particle size was 30.33 nm as calculated from XRD patterns for (Co, Cu)/ZnO. UV-Vis absorption spectrum indicates that the co-doped ZnO exhibits increased visible light absorption compared to the undoped one. The photoluminescence spectroscopy shows that the separation efficiency of photo-induced electrons and hole is enhanced by the co-doping strategy. (Co, Cu)/ZnO nanoparticles demonstrated a strong visible light response and high photocatalytic activity for Rhodamine B (RhB) degradation under irradiation by visible light (400-500 nm). The visible-light photocatalytic activity of the prepared (Co, Cu)/ZnO may come about because of the incorporation of Co, Cu atoms in ZnO, photo-induced electron-hole pairs and extended the spectral response to the visible region. The antibacterial and antifungal activities of ZnO, Co-ZnO, Cu-ZnO, and (Co, Cu)/ZnO were studied respectively with *Staphylococcus aureus* (Gram-positive), *Escherichia coli* (Gram-negative) (bacterial strain) and *Aspergillus flavus*, *Candida albicans* (fungal strain). The (Co, Cu)/ZnO enhanced the antimicrobial activity.

Keywords: *(Co, Cu)/ZnO nanoparticles, antimicrobial activity, photocatalysis, Rhodamine B*

How to cite this article
Sheik Muhideen Badhusha M., Kavitha B., Rajarajan M., Tharmaraj P., Suganthi A. Synthesis of Co and Cu codoped ZnO nanoparticles by citrate gel combustion method: Photocatalytic and antimicrobial activity. J. Water Environ. Nanotechnol., 2022; 7(2): 143-154.
DOI: 10.22090/jwent.2022.02.003

INTRODUCTION

Industrial wastewater contains organic pollutants and disease-causing microbial pathogens. Rhodamine B is one of the famous dyes that is involved extensively as a dye laser substance and in the textiles industry owing to its high stability. Thereby, the removal of this harmful dye is viewed as one of the important challenges in recent years by utilizing a simple and low costs process [1– 4]. Many conventional chemical, electrochemical and biological treatment methods were limited because of low degradation efficiency, consumption of chemicals, and generation of the second pollution. The photocatalytic processes on semiconducting materials have been extensively used in the fields of environmental applications such as water disinfection, hazardous waste remediation, and water purification [5]. Especially, photocatalytic degradation of organic pollutants under visible irradiation continues to expand research interests [6-8]. As for the most popular photocatalysts, TiO_2 and ZnO, their photocatalytic activities entirely

* Corresponding Author Email: *rajarajanchem1962@gmail.com*
ptharma@rediffmail.com

depend on ultraviolet irradiation due to the wide band gap of about (3.37 eV), which results in low efficiency in utilizing solar energy [9]. Although modified ZnO by doping diverse metals [10] and nonmetals [11, 12] may show improved sensitivity toward the visible light region through the narrowing of the band gap energy. The transition metal ion doping could reduce the energy for band gap excitation and the recombination rate of photo-generated electron-hole pairs, thus improving photocatalytic efficiency under visible light.

Sankara reddy et al. reported that silver and cobalt co-doped ZnO nanoparticles display excellent antibacterial activity than the Ag-doped, Co-doped, and undoped ZnO nanoparticles [13]. Vignesh et al examined al studied the visible light-assisted photocatalytic performance of Ni and Th co-doped ZnO nanoparticles for the degradation of methylene blue dye. Ni–Th–ZnO possesses excellent photocatalytic activity for the degradation of MB when compared to that of Ni–ZnO, Th–ZnO, ZnO, and TiO_2 [14]. . Lakshmi Narayana et al investigated the photocatalytic degradation of basic green dye by pure and Fe, Co-doped TiO_2 under daylight illumination [15]. The previous research reported that two dopants had a more synergistic effect than a single one for enhancing the absorption in the visible-light region and improving the photocatalytic activity of ZnO [16 - 18]. Doping is the way of adding controlled impurities to a semiconductor material which causes significant changes in its physical, chemical, and biological properties. Metals have been used to create doped ZnO semiconductors. . Most of the studies describe the photoluminescence, optical and magnetic properties of the ZnO semiconductors [19- 21]. Among these different metallic doping elements, Co and Cu are important because, they are prominent luminescence activators, which can alter the luminescence of ZnO crystal by making localized impurity levels. Likewise, it can change the microstructure and the optical properties of ZnO [22].

The synthesis technique alters the material's surface shape, resulting in a change in photocatalytic activity. Sol-gel synthesis, hydrothermal synthesis, electrochemical, chemical vapor deposition, co-precipitation, magnetron sputtering, and citrate gel combustion are some of the methods used to make ZnO-based nanostructured materials. For the manufacture of nanocrystalline ZnO powders, low-temperature combustion methods have proven to be particularly beneficial. These chemical synthesis processes have several advantages, including superior stoichiometric control and the ability to produce ultra-fine particles with a narrow size distribution in a short amount of time. To the best of our knowledge, the production of (Co, Cu)/ZnO nanoparticles based photocatalyst by citrate gel combustion has not been reported in the literature.

The present examination focuses on a novel citrate-gel combustion strategy to synthesize single doping, such as Co-ZnO, Cu-ZnO, and codoped (Co, Cu)/ZnO nanoparticles. The microstructure and morphology of samples were characterized by UV-Vis-DRS, FT-IR, XRD, PL, SEM, and EDX. The photocatalytic activities of the degradation of Rhodamine-B (Rh-B) under visible light irradiation were assessed and the antimicrobial activity against pathogenic bacteria and fungi was studied.

EXPERIMENTAL

Materials

Rhodamine B, zinc sulfate, copper sulfate pentahydrate ($CuSO_4.5H_2O$), cobaltous sulfate monohydrate ($CoSO_4.9H_2O$), citric acid ($C_6H_8O_7$), and ethanol (Merck) were utilized of analytical grade. Double distilled water was utilized in all photocatalytic experiments.

Synthesis of ZnO, Co-ZnO, Cu-ZnO, and (Co, Cu)/ ZnO nanoparticles

ZnO, Co-ZnO, Cu-ZnO and (Co, Cu)/ZnO nanostructures were prepared by citrate gel route. A stoichiometric amount of zinc sulfate along with citric acid ($C_6H_8O_7$) was dissolved in 100 ml of ethanol, for Co and Cu dopants 5 mol% of cobaltous sulfate and copper sulfate have been added drop-wise individually and combinedly to the above solution under continuous stirring for 5 h to make a sol which was then placed in an oven for 12 h at 95 °C to form a gel. The gel was then sintered at 673 K for 3 h and was ground to produce fine powder [23, 24].

Characterization

The UV-vis-DRS spectral measurements were performed with a JASCO V-550 double beam spectrophotometer with a PMT detector. . The FTIR spectra of the samples have been recorded utilizing Perkin Elmer IR spectrophotometer with KBr plates over the range 4000 – 400 cm^{-1}. The crystal structure of the samples has been examined utilizing XPERT PRO X-Ray diffractometer with

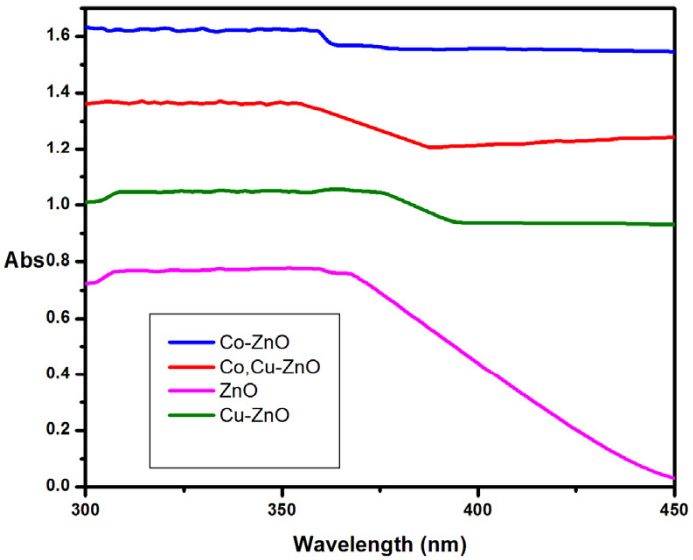

Fig. 1. UV- DRS spectrum of Co and Cu codoped ZnO nanoparticles

Cu K α radiation of wavelength 1.541 Aº and scanning angle 2θ extending from 10º to 80º. The average crystallite size is determined by applying the Debye-Scherrer formula:

$$D = \frac{0.89\lambda}{\beta \cos\theta} \quad (1)$$

Where D is the average crystallite size, β is the full-width half maximum (FWHM) of the 2θ peak, K is the shape of the factor of the particles (it equals 0.89), θ and λ are the incident of angle and wavelength of the X-rays, respectively. Scanning electron microscopy (SEM) observations were performed using a JSM 6701F-6701 instrument in both secondary and backscattered electron modes. The elemental analysis was studied by energy-dispersive X-ray spectroscopy (EDS) attached to the SEM. The photoluminescence spectra were recorded using a spectrofluorometer (JASCO-FP-6200) at room temperature. The photoluminescence spectroscopy was used to measure the emission characteristics of doped and undoped ZnO nanoparticles.

Procedure for evaluation of photocatalytic activity

300 mL of RhB solution with an initial concentration of 5 µM was taken in a cylindrical glass vessel. It was encompassed by a circulating water jacket to cool the lamp. Air was persistently bubbled into the aliquot using an air pump to provide a constant source of dissolved oxygen. At that point, the photocatalyst was added to the vessel. Before illumination, the aqueous suspension was continuously stirred for 30 min in dark to reach adsorption-desorption equilibrium [25] [23]. The mixture was subjected to visible irradiation and the source of visible light was 300 W Xe-arc lamps with a UV-cut-off filter. During irradiation, 5 mL of aliquot samples were withdrawn from the reaction mixture at a regular time interval of 30 min. The sampled suspensions were centrifuged at 4000 rpm for 20 min to remove the catalyst and the residual RhB concentration was analyzed by UV-vis spectrophotometer at 554 nm. The degradation efficiency (%) was calculated as follows:

$$\textbf{Degradation efficiency (\%)} = \frac{C0 - C}{C0} \times 100 \quad \textbf{(2)}$$

Where C_0 is the initial concentration of RhB and C is the concentration of RhB after a certain irradiation time. Chemical oxygen demand (COD) experiments were performed by the dichromate oxidation method, after the completion of photodegradation.

Antimicrobial experimentation

The Antimicrobial activity of synthesized nanoparticles was examined against *Staphylococcus aureus* (Gram-positive), Escherichia *coli* (Gram-negative), *Aspergillus flavus, and Candida albicans* (Antifungal activity). The antimicrobial assays were performed by well diffusion method in Muller Hinton Agar plate at a concentration of 10 mg/ml. The results of the in-vitro antimicrobial activities

were recorded as the average diameter of the inhibition zone in mm which is given in Table. 3.

RESULTS AND DISCUSSION

Characterization

UV-vis-DRS

The UV-vis-DRS of ZnO, Co-ZnO, Cu-ZnO, and (Co, Cu)/ZnO nanostructures are shown in Fig. 1. The absorption edges of doped (Co, Cu)/ZnO are red-shifted when compared to that of ZnO. The optical band gaps are determined using the Tauc equation [26] [24]:

$$\alpha = \frac{C(h\upsilon - E_g^{bulk})^2}{h\upsilon} \quad (3)$$

Where α, C, hυ, and E_g^{bulk} are absorption coefficients, constant, photon energy, and band gap respectively. Tauc plots of ZnO, Co-ZnO, Cu-ZnO, and (Co, Cu)/ZnO nanostructures are given in Fig. 2. The optical band gaps are found to be 3.0 eV, 2.9 eV, 3.28 eV, and 2.64 eV for ZnO, Cu-ZnO, Co-ZnO, and (Co, Cu)/ZnO nanostructures respectively. Compared with the samples ZnO, Co-ZnO, Cu-ZnO and (Co, Cu)/ZnO the band gap energy of (Co, Cu)/ZnO decreased moderately. The result indicates that the (Co, Cu) doping on ZnO leads to the band gap narrowing and responds to the visible light degradation of Rhodamine B.

XRD

The XRD patterns of ZnO, Co-ZnO, Cu-ZnO, and (Co, Cu)/ZnO nanostructures are shown in Fig. 3. The pronounced diffraction peaks in the XRD pattern clearly show the crystalline nature with sharp peaks corresponding to (100), (002), (101), (102), (110), (103), (200), (112) and (201) planes. It is discovered that all the significant diffraction peaks can be perfectly indexed with standard (phase: hexagonal; lattice: primitive; JCPDS 36-1451). In conclusion, co-doping does not modify the crystallographic structure of ZnO [27] [25]. The crystallite sizes were determined as 38.71 nm, 44.02 nm, 39.38 nm, and 30.33 nm for ZnO, Co-ZnO, Cu-ZnO, and (Co, Cu)/ZnO nanoparticles respectively. Since Co and Cu doping can suppress its crystal growth. It has been reported that ZnO doped with transition metals such as Co and Cu possesses a smaller particle size. The decrease in crystal size is due to the doping of Co and Cu [28] [26].

FT-IR

Fig. 4 shows the FT-IR spectra of the ZnO, Co-ZnO, Cu-ZnO, and (Co, Cu)/ZnO nanoparticles

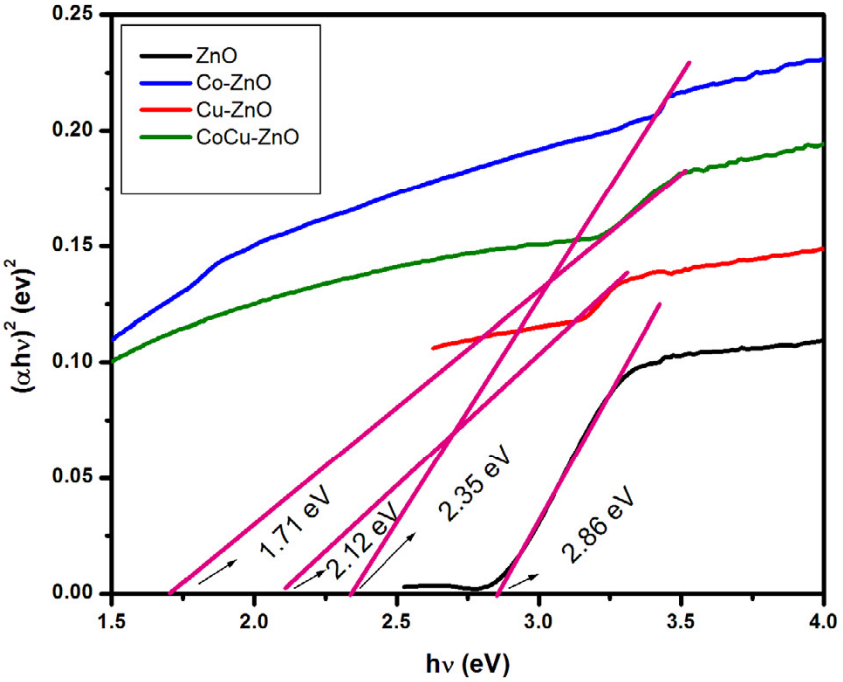

Fig. 2. Tauc plot of ZnO,Co-ZnO, Cu-ZnO and (d) CoCu-ZnO nanoparticles

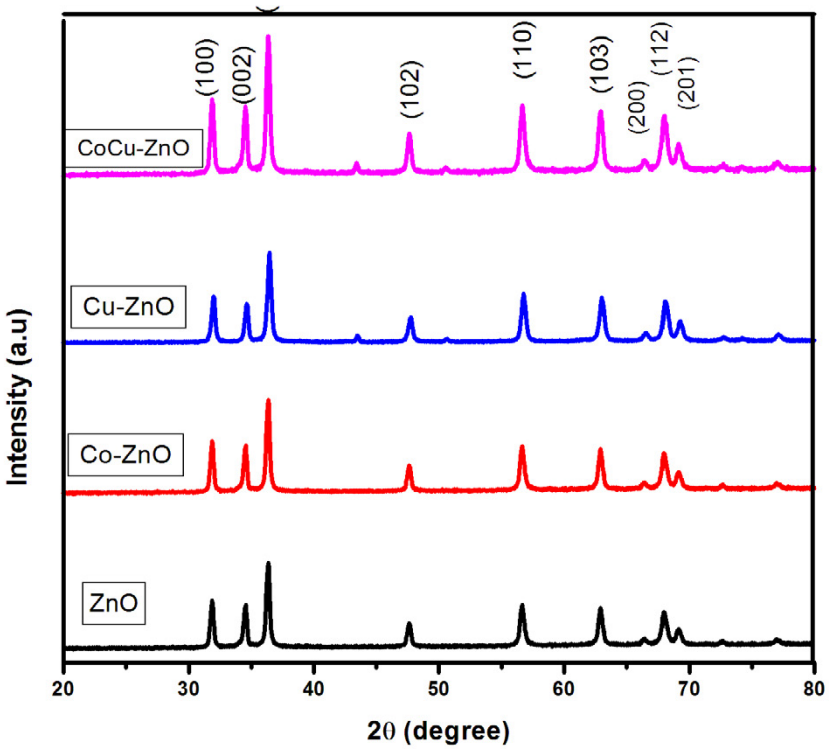

Fig. 3. XRD patterns of ZnO, Cu-ZnO, Co-ZnO and (Co, Cu)/ZnO

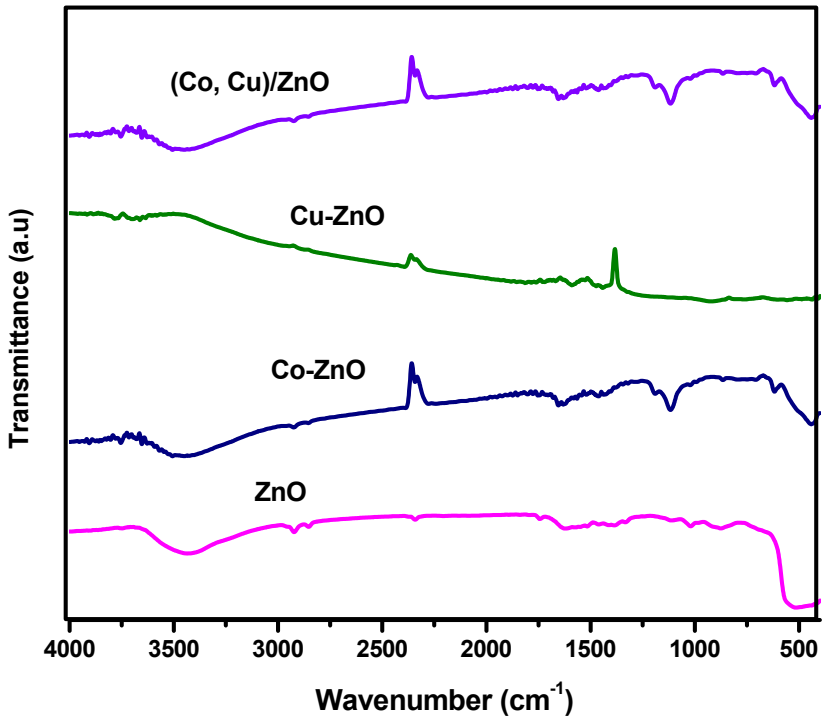

Fig. 4. FTIR spectrum of ZnO, Cu-ZnO, Co-ZnO and (Co, Cu)/ZnO

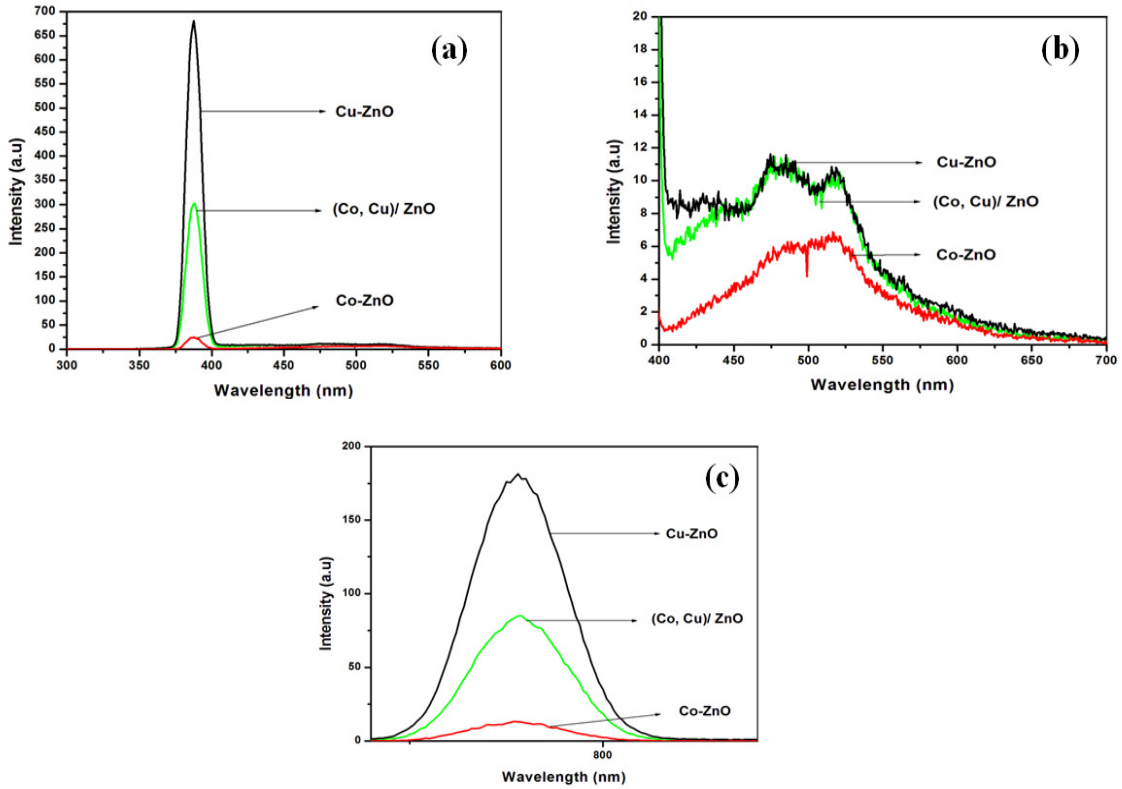

Fig. 5. PL spectra of ZnO, Cu-ZnO, Co-ZnO and (Co, Cu)/ZnO nanoparticles at (a) 385nm; (b) 520 nm; (c) 790 nm

respectively. In Fig. 4, an intense band at 3491 cm^{-1} proposes the presence of non-dissociated OH groups of citric acid (CA). The peak around 2918 cm^{-1} is due to CH_2 stretching, peak at 1653 cm^{-1} may be assigned to the symmetric stretching of OH from the COOH group, displaying the binding of a citric acid radical to the ZnO surface. The 1755 cm^{-1} peak of CA, is attributable to the C = O vibration from the COOH group of CA. This peak shifts to an intense band at about 1653 cm^{-1} for ZnO - CA, displaying the binding of a CA radical to the surface of ZnO nanoparticles by chemisorptions of carboxylate (citrate) ions [29]. Carboxylate groups of CA form complexes with Zn atoms on the surface of ZnO representing a partial single bond character to the C = O bond. The next band at 1389 cm^{-1} can be allocated to the asymmetric stretching of CO from the COOH group. The broad absorption peaks at 3460 cm^{-1} for ZnO nanoparticles are attributed to polymeric O-H stretching vibration of H_2O in Zn-O lattice [30] [27] which is shifted to 3500 cm^{-1} for doped ZnO nanoparticles. The appearance of a sharp band at 449 cm^{-1} represents the stretching mode of Zn-O [31] which is shifted to a higher frequency as 452 cm^{-1} for doped ZnO nanoparticles.

PL spectra

photoluminescence (PL) studies are also a powerful method for exploring the impact of doping on the optical properties of semiconductor nanostructures with direct band gaps because doping nanostructures are expected to have different optical properties compared to undoped nanostructures. As demonstrated in Fig. 5, photoluminescence (PL) studies were conducted to investigate its emission properties. The photoluminescence of synthesized materials revealed three emission bands: one blue band at 385 nm, a possible green band at 520 nm, and a red band at roughly 790 nm. The PL of the samples in our case differs significantly from that of ZnO crystals, which typically display UV emission at 385 nm due to radiative recombination between electrons in the conduction band and holes in the valence band and the holes in the valence band. The green band at 520 nm and the red band at 790 nm could be linked to a transition

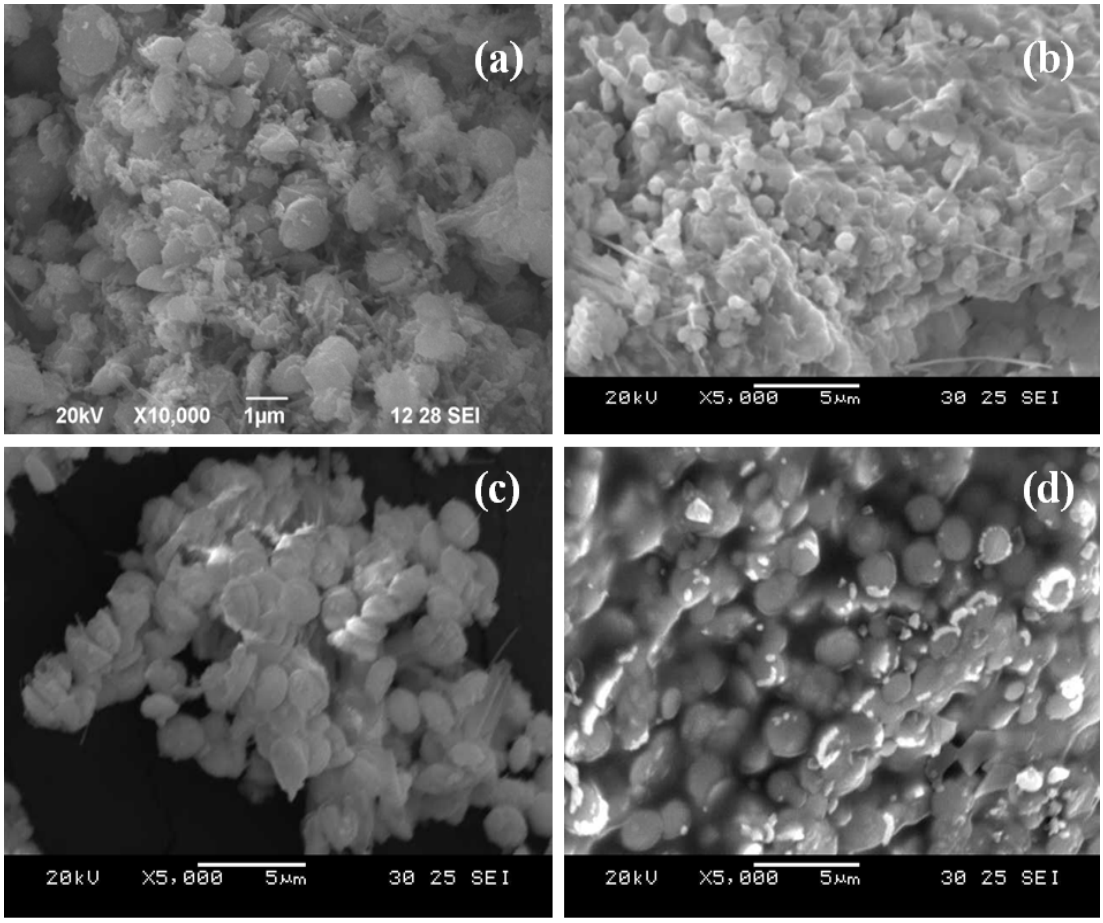

Fig. 6. SEM image of (a) ZnO; (b) Cu-ZnO; (c) Co-ZnO and (d) (Co, Cu)/ZnO

between oxygen vacancy and interstitial oxygen. The recombination of photo-induced charge carriers produces the photoluminescence (PL) spectra of semiconductors. The PL spectra can be used to analyze electron/hole pair transport and recombination. [32] .

Therefore, a decrease in PL intensity reduces the recombination rate of photo-induced electron-hole pairs. The PL intensity decreases sharply in the following order: ZnO < Co-ZnO < Cu-ZnO < (Co,Cu)/ZnO. PL intensity of the UV emission peak decreases because the crystallization of the samples is poorer and poorer. A dominant ultraviolet (UV) emission and a weak visible emission can be detected for all the samples, which can be identified as the excitonic emission and defect-related emission, respectively. However, as the surface-related defects were depressed, the visible emissions of the ZnO nanoparticles doped with Co and Cu are higher than that of ZnO.

SEM and EDX

The surface morphologies of ZnO, Co-ZnO, Cu-ZnO, and (Co, Cu)/ZnO nanostructures are characterized by SEM and are shown in Fig. 6 (a), (b), (c), and (d). The (Co, Cu) doped ZnO has spherical-like morphology, a smaller particle size, and also the nanoparticles are slightly agglomerated. From Fig 6 (d), it was observed that the average crystalline size was found to be 27-35 nm which is in good agreement with the XRD results.

The energy dispersive X-ray spectrum (EDX) is used to analyze the (Co, Cu)/ZnO nanostructure and the results are tabulated (Table. 1). Co, Cu, Zn, and O peaks are formed in the spectrum, confirming the formation of (Co, Cu)/ZnO nanostructures (Fig. 7).

Photocatalytic activity

Photodegradation of RhB

Photocatalytic tests were done with an

Table. 1 EDX elemental analysis of Co-Zno, Cu-ZnO and (Co, Cu)/ ZnO

Sample name	Atomic (%)	KeV
ZnO	O = 66.60 Zn = 33.40	O = 0.52, Zn = 1.01, 8.63, 9.57
Co-ZnO	O = 74.05 Zn = 24.43 Co = 1.52	O = 0.52 Zn = 1.01, 8.63, 9.57 Co = 0.85, 7.47, 8.26
Cu-ZnO	O = 74.05 Zn = 24.43 Cu = 1.52	O = 0.52 Zn = 1.01, 8.63, 9.57 Cu = 0.85, 7.47, 8.26
(Co, Cu)/ ZnO	O = 74.05 Zn = 22.91 Co = 1.52 Cu =1.52	O = 0.52 Zn = 1.01, 8.63, 9.57 Co = 0.85, 7.47, 8.26 Cu = 2.32, 3.14, 3.37

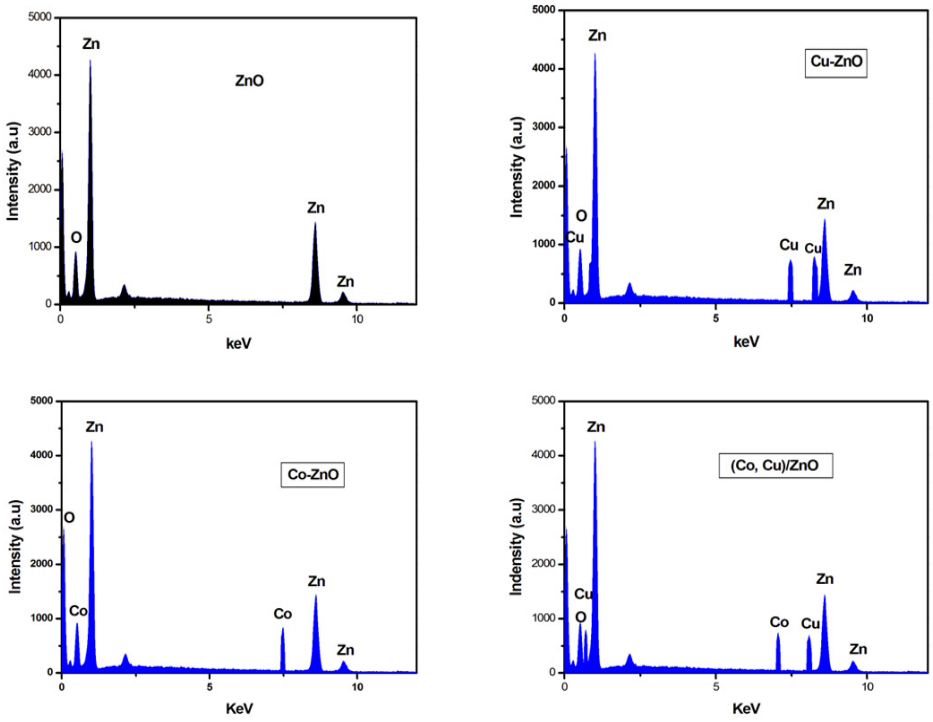

Fig. 7. EDX spectrum of ZnO; Cu–ZnO; Co–ZnO and (Co, Cu)/ZnO

underlying RhB concentration of 5 μM, catalyst concentration of 0.12 g/L, pH 10, and illumination time of 180 min. Fig. 8. (a) demonstrates the adjustment in absorption spectra of RhB presented to visible light for different irradiation times (0 min, 30 min, 60 min, 90 min, 120 min, 150 min, and 180 min) within the sight of (Co, Cu)/ZnO. The absorption maxima at 554 nm decreased gradually with an extension of irradiation time.

The examination of photodegradation and COD expulsion level of RhB over ZnO, Co– ZnO, Cu– ZnO, and (Co, Cu)/ZnO have appeared in Fig. 8. (b). The outcomes uncover that the metal-doped ZnO indicated higher photocatalytic action than that of ZnO. (Co, Cu)/ZnO demonstrated momentous photograph reactant movement with degradation of 98% and COD evacuation of 70.51% for RhB. The expansion in evacuation level of COD affirms the mineralization of RhB amid photodegradation. In this manner, doping of Co and Cu in ZnO fundamentally enhances its photocatalytic action by improving the electron–opening detachment on the photocatalyst surface. The photodegradation efficiencies of RhB utilizing ZnO, Co– ZnO, Cu– ZnO, and (Co, Cu)/ZnO have appeared in Fig. 8. (c). The removal percentage of

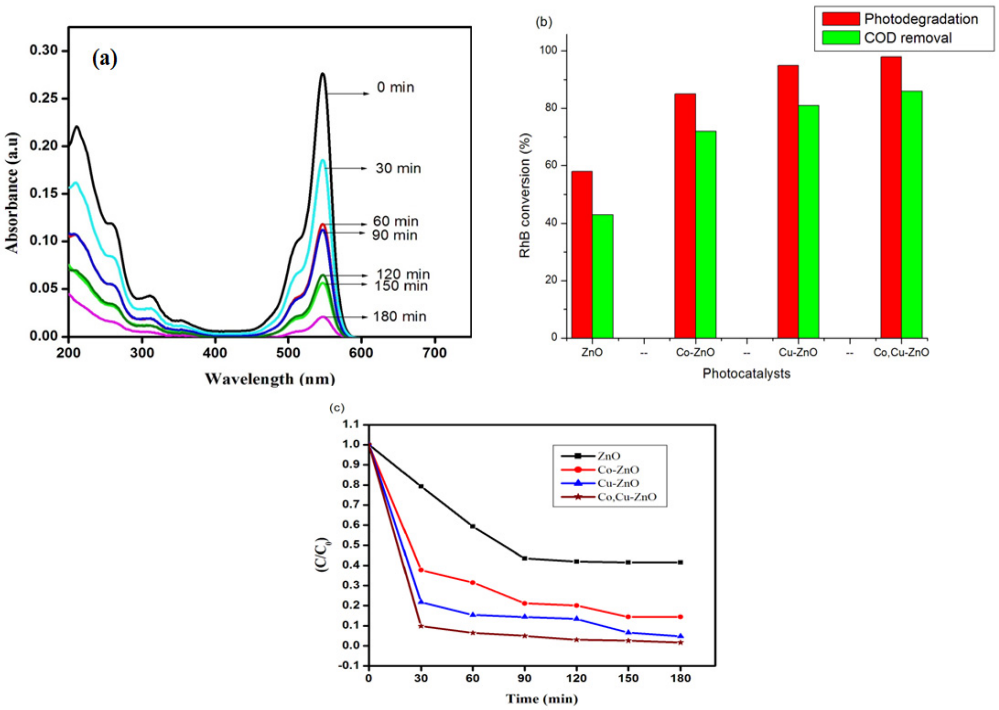

Fig. 8. (a) Time-dependent UV–vis spectral changes of RhB (5μM) in the presence of (Co, Cu)/ZnO (0.12 g/L) under visible light irradiation; (b) Comparison of photodegradation and COD removal percentage of RhB in the presence ZnO, Co–ZnO, Cu–ZnO and (Co, Cu)/ZnO and (c) Degradation of RhB as a function of irradiation time in the presence of ZnO, Co-ZnO, Cu-ZnO and Co, Cu codoped ZnO
[reaction conditions: pH = 10; RhB concentration = 5 μM; catalyst dosage = 0.12 g/L and irradiation time = 180 min]

Table. 2. Comparison of the degradation efficiency with other catalysts for RhB

Catalyst Name	Dye	% Degradation	Reference
Co_3O_4	RhB	90 %	[30]
ZnO	RhB	95 %	[31]
F-MWCNTs/Co–Ti oxide	RhB	93.35%	[32]
C, N-TiO_2	RhB	94%	[33]
NiO	RhB	80.33%	[34]
(Co, Cu)/ ZnO	RhB	98 %	Present Study

RhB with different catalysts is presented in Table 2 [33 – 37].

Mechanism of degradation of Rhodamine B

The impurity band exists in the middle of the optical band gap of doped ZnO. In these investigations under visible light illumination, the electrons can exchange from the valence band to their purity band by absorbing photons (λ > 400 nm), and the electrons in the impurity band would then be able to exchange to the high-energy express (the conduction band) by engrossing different photons (Fig. 9). In this procedure, likely, a few electrons exchanging to the conduction band come straightforwardly from the impurity band as opposed to from the valence band. The examples of the conduction band electrons (e^-) and valence band hole (h^+) develop after two advances, and they can relocate toward the ZnO surface [38]. ZnO can be energized by implication through RhB, the response with oxygen prompts the development of $O_2^{-\bullet}$. From ensuing responses after the arrangement of the superoxide particle, hydroxyl radicals are shaped. The arrangement of $OH^\bullet$ is essential for the debasement of RhB and subsequently required for the total corruption of RhB.

The plausible reaction pathways are:

$$ZnO + hv \rightarrow ZnO (e^-_{CB} + h^+_{VB}) \quad 1$$

$$Co^{2+} + hv \rightarrow e^- + Co^{3+} \quad 2$$

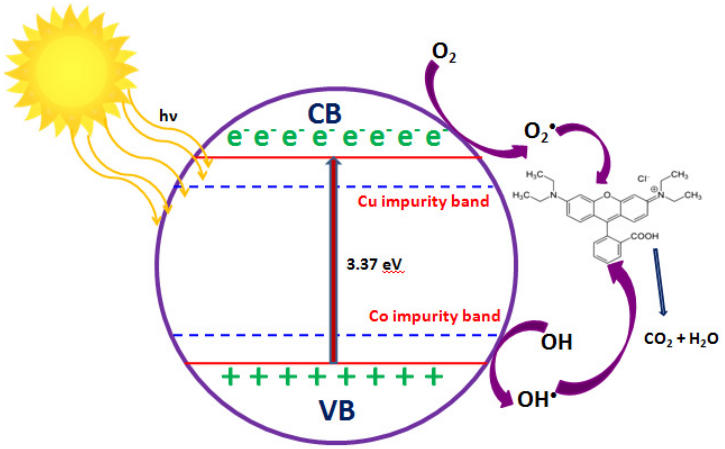

Fig. 9. Schematic illustration of the modification of ZnO due to metal doping as impurities

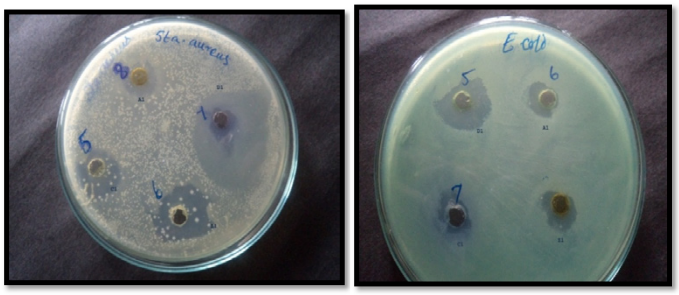

Fig. 10. Antibacterial activity of ZnO, Co-ZnO, Cu-ZnO and (Co, Cu)/ ZnO Nps against *Staphylococcus aureus and Escherichia coli*

$$Cu^{+} + h\nu \rightarrow e^{-} + Cu^{2+} \quad (3)$$

$$ZnO + RhB^{*} \rightarrow RhB^{+\bullet} + ZnO(e^{-}) \quad (4)$$

$$ZnO\ (e^{-}) + O_2 \rightarrow ZnO + O_2^{-\bullet} \quad (5)$$

$$ZnO(e^{-}) + O_2^{-\bullet} + H^{+} \rightarrow HO_2^{-} + ZnO \quad (6)$$

$$HO_2^{-} + H^{+} \rightarrow H_2O_2 \quad (7)$$

$$H_2O_2 + e^{-} \rightarrow OH^{\bullet} + OH^{-} \quad (8)$$

Anti-microbial activity

Fig. 10 shows the maximum inhibitory effect of ZnO, Co-ZnO, Cu-ZnO, and (Co, Cu)/ ZnO nanostructures against *E. coli* and *S. areus*. Table. 3 indicates the increasing antimicrobial activity against bacterial and fungal strains by the maximum zone of inhibition, Fig. 11 records the maximum inhibitory effect of ZnO, Co-ZnO, Cu-ZnO, and (Co, Cu)/ZnO nanostructures against *A. flavus* and *C. albicans*.

CONCLUSION

ZnO, Co-ZnO, Cu-ZnO, and (Co, Cu)/ZnO nanoparticles were synthesized by a novel citrate gel method. The samples have been characterized by UV-Vis DRS, XRD, FTIR, SEM EDAX, and PL analysis. The XRD and SEM results reveal that the crystal structure and morphology are not affected by the doping (Co and Cu) ZnO. The photocatalytic activity was examined by the degradation of RhB and the activity of photocatalyst in the following order: ZnO < Co-ZnO < Cu-ZnO < (Co, Cu)/ZnO. The prepared (Co, Cu)/ZnO nanoparticles display good absorption of visible light making a redshift. The red shift is the consequence of the band gap decrease resulting from the impurity band in the middle of the optical band gap of ZnO. The recombination rate of the photo-induced electron-hole pairs is decreased because of Co and Cu codoping and the efficiency of photodegradation is enhanced under visible light irradiation. The zone of inhibition was found against pathogenic bacteria and fungal strains and it confirms that the co-doped

Table. 3 Antimicrobial activity of ZnO, Cu-ZnO, Co-ZnO and (Co, Cu)/ ZnO NPs against pathogenic bacterial and fungal strains

Type of nanoparticles	Diameter of inhibition zone (mm)		Diameter of inhibition zone (mm)	
	Bacterial strains		Fungal strains	
	Staphylococcus aureus	*Escherichia coli*	*Aspergillus flavus*	*Candida albicans*
ZnO	13	13	12	11
$Zn_{0.95}Co_{0.05}O$	15	14	14	13
$Zn_{0.95}Cu_{0.05}O$	15	14	14	13
$Zn_{0.95}Co_{0.05}Cu_{0.05}O$	19	15	17	14

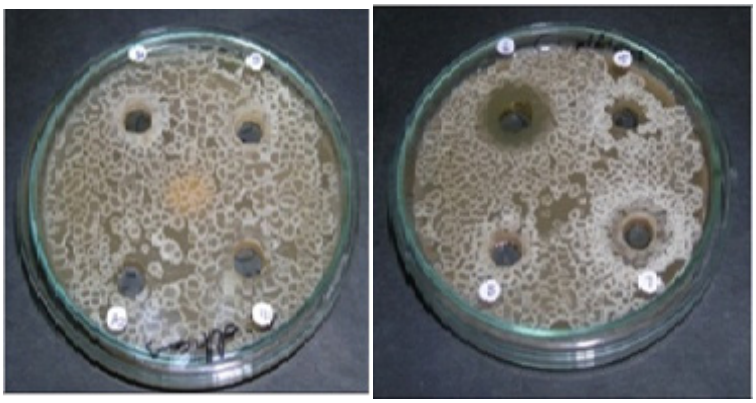

Fig. 11 Antifungal activity of ZnO, Co-ZnO, Cu-ZnO and (Co, Cu)/ ZnO Nps against *Aspergillus flavus and Candida albicans*

(Co, Cu)/ ZnO display an excellent antibacterial and antifungal activity than the Co-ZnO and Cu-ZnO. Hence, Co and Cu co-doped ZnO are identified as promising antimicrobial agents. Thus, the present study indicates that Co-doped ZnO can potentially be used in food preservation, water purification, and pharmaceuticals to prepare anti-drug agents.

CONFLICT OF INTEREST

The authors declare no conflict of interest.

REFERENCES

[1] Akpan, U. G., & Hameed, B. H. (2009). Parameters affecting the photocatalytic degradation of dyes using TiO2-based photocatalysts: a review. Journal of hazardous materials, 170(2-3), 520-529. https://doi.org/10.1016/j.jhazmat.2009.05.039

[2] Díaz-Cruz, M. S., & Barceló, D. (2008). Trace organic chemicals contamination in ground water recharge. Chemosphere, 72(3), 333-342. https://doi.org/10.1016/j.chemosphere.2008.02.031

[3] Merouani, S., Hamdaoui, O., Saoudi, F., & Chiha, M. (2010). Sonochemical degradation of Rhodamine B in aqueous phase: effects of additives. Chemical Engineering Journal, 158(3), 550-557. https://doi.org/10.1016/j.cej.2010.01.048

[4] Natarajan, T. S., Thomas, M., Natarajan, K., Bajaj, H. C., & Tayade, R. J. (2011). Study on UV-LED/TiO2 process for degradation of Rhodamine B dye. Chemical Engineering Journal, 169(1-3), 126-134. https://doi.org/10.1016/j.cej.2011.02.066

[5] Kim, C., Choi, M., & Jang, J. (2010). Nitrogen-doped SiO2/TiO2 core/shell nanoparticles as highly efficient visible light photocatalyst. Catalysis Communications, 11(5), 378-382. https://doi.org/10.1016/j.catcom.2009.11.005

[6] Shao, M., Cheng, L., Zhang, X., Ma, D. D. D., & Lee, S. T. (2009). Excellent photocatalysis of HF-treated silicon nanowires. Journal of the American Chemical Society, 131(49), 17738-17739. https://doi.org/10.1021/ja908085c

[7] Gopal, N. O., Lo, H. H., & Ke, S. C. (2008). Chemical state and environment of boron dopant in B, N-codoped anatase TiO2 nanoparticles: an avenue for probing diamagnetic dopants in TiO2 by electron paramagnetic resonance spectroscopy. Journal of the American Chemical Society, 130(9), 2760-2761. https://doi.org/10.1021/ja711424d

[8] Hu, C., Peng, T., Hu, X., Nie, Y., Zhou, X., Qu, J., & He, H. (2010). Plasmon-induced photodegradation of toxic pollutants with Ag– AgI/Al2O3 under visible-light irradiation. Journal of the American Chemical Society, 132(2), 857-862. https://doi.org/10.1021/ja907792d

[9] Thompson, T. L., & Yates, J. T. (2006). Surface science studies of the photoactivation of TiO2 new photochemical processes. Chemical reviews, 106(10), 4428-4453. https://doi.org/10.1021/cr050172k

[10] Choi, W., Termin, A., & Hoffmann, M. R. (2002). The role of metal ion dopants in quantum-sized TiO2: correlation between photoreactivity and charge carrier recombination dynamics. The Journal of Physical Chemistry, 98(51), 13669-13679. https://doi.org/10.1021/j100102a038

[11] Sakthivel, S., Janczarek, M., & Kisch, H. (2004). Visible light activity and photoelectrochemical properties of nitrogen-doped TiO2. The Journal of Physical Chemistry B, 108(50), 19384-19387. https://doi.org/10.1021/jp046857q

[12] Sato, S., Nakamura, R., & Abe, S. (2005). Visible-light sensitization of TiO2 photocatalysts by wet-method N doping. Applied Catalysis A: General, 284(1-2), 131-137. https://doi.org/10.1016/j.apcata.2005.01.028
[13] Reddy, S., Reddy, V., Reddy, K., & Kumari, P. (2013). Synthesis, structural, optical properties and antibacterial activity of co-doped (Ag, Co) ZnO nanoparticles. Research Journal of Material Sciences, 1(1), 11-20.
[14] Vignesh, K., Rajarajan, M., & Suganthi, A. (2014). Visible light assisted photocatalytic performance of Ni and Th co-doped ZnO nanoparticles for the degradation of methylene blue dye. Journal of Industrial and Engineering Chemistry, 20(5), 3826-3833. https://doi.org/10.1016/j.jiec.2013.12.086
[15] Narayana, R. L., Matheswaran, M., Abd Aziz, A., & Saravanan, P. (2011). Photocatalytic decolourization of basic green dye by pure and Fe, Co doped TiO2 under daylight illumination. Desalination, 269(1-3), 249-253. https://doi.org/10.1016/j.desal.2010.11.007
[16] Lan, M., Fan, G., Sun, W., & Li, F. (2013). Synthesis of hybrid Zn-Al-In mixed metal oxides/carbon nanotubes composite and enhanced visible-light-induced photocatalytic performance. Applied surface science, 282, 937-946. https://doi.org/10.1016/j.apsusc.2013.06.095
[17] Lu, S. X., Zhu, T., & Xu, W. G. (2009, September). Enhanced photocatalytic properties of quantum-sized ZnO induced by La3+-Nd3+ co-doping. In Journal of Physics: Conference Series (Vol. 188, No. 1, p. 012007). IOP Publishing. https://doi.org/10.1088/1742-6596/188/1/012007
[18] Kaneva, N. V., Dimitrov, D. T., & Dushkin, C. D. (2011). Effect of nickel doping on the photocatalytic activity of ZnO thin films under UV and visible light. Applied Surface Science, 257(18), 8113-8120. https://doi.org/10.1016/j.apsusc.2011.04.119
[19] Soares, J. W., Whitten, J. E., Oblas, D. W., & Steeves, D. M. (2008). Novel photoluminescence properties of surface-modified nanocrystalline zinc oxide: toward a reactive scaffold. Langmuir, 24(2), 371-374. https://doi.org/10.1021/la702834w
[20] Viswanatha, R., Nayak, Y. A., Venkatesha, T. G., & Vidyasagar, C. C. (2013). Synthesis, characterization and optical properties of Sn-ZnO nanoparticle. Nanoscience and Nanotechnology, 3(1), 16-20.
[21] Xu, H., Zhao, Q., Yang, H., & Chen, Y. (2009). Study of magnetic properties of ZnO nanoparticles codoped with Co and Cu. Journal of Nanoparticle Research, 11(3), 615-621. https://doi.org/10.1007/s11051-008-9444-6
[22] Muthukumaran, S., & Gopalakrishnan, R. (2012). Structural, optical, FTIR and photoluminescence properties of Zn0. 96− xCo0. 04CuxO (x= 0.03, 0.04 and 0.05) nanopowders. Physica B: Condensed Matter, 407(17), 3448-3456. https://doi.org/10.1016/j.physb.2012.04.057
[23] Nitthaisong, A., Charojrochkul, S., & Kuharuangrong, S. (2017). Effect of Cu-Doped ZnO Sorbents for Desulfurization. In Key Engineering Materials (Vol. 728, pp. 335-340). Trans Tech Publications Ltd. https://doi.org/10.4028/www.scientific.net/KEM.728.335
[24] Ananthakumar, S., Mangalaraja, R. V., Ambily, J., & Anas, S. (2010). Microwave assisted citrate gel combustion synthesis of ZnO Part-I: assessment of structural features.
[25] Vignesh, K., Suganthi, A., Rajarajan, M., & Sara, S. A. (2012). Photocatalytic activity of AgI sensitized ZnO nanoparticles under visible light irradiation. Powder technology, 224, 331-337. https://doi.org/10.1016/j.powtec.2012.03.015
[26] Kang, H. S., Kang, J. S., Kim, J. W., & Lee, S. Y. (2004). Annealing effect on the property of ultraviolet and green emissions of ZnO thin films. Journal of Applied Physics, 95(3), 1246-1250. https://doi.org/10.1063/1.1633343
[27] Vignesh, K., Suganthi, A., Rajarajan, M., & Sakthivadivel, R. (2012). Visible light assisted photodecolorization of eosin-Y in aqueous solution using hesperidin modified TiO2 nanoparticles. Applied surface science, 258(10), 4592-4600. https://doi.org/10.1016/j.apsusc.2012.01.035
[28] Song, J. L., Zheng, J. H., Zhen, Z. H. A. O., Zhou, B. Y., & Lian, J. S. (2013). Synthesis and photoluminescence of Y and Cd co-doped ZnO nanopowder. Transactions of Nonferrous Metals Society of China, 23(8), 2336-2340. https://doi.org/10.1016/S1003-6326(13)62738-7
[29] Manoharan, D., & Vishista, K. (2013). Optical properties of nano-crystalline cerium dioxide synthesized by single step aqueous citrate-nitrate gel combustion method. Asian Journal of Chemistry, 25(16), 9045. https://doi.org/10.14233/ajchem.2013.14984
[30] Muthukumaran, S., & Gopalakrishnan, R. (2012). Structural, FTIR and photoluminescence studies of Cu doped ZnO nanopowders by co-precipitation method. Optical Materials, 34(11), 1946-1953. https://doi.org/10.1016/j.optmat.2012.06.004
[31] Hernández, A., Maya, L., Sánchez-Mora, E., & Sánchez, E. M. (2007). Sol-gel synthesis, characterization and photocatalytic activity of mixed oxide ZnO-Fe2O3. Journal of Sol-Gel Science and Technology, 42(1), 71-78. https://doi.org/10.1007/s10971-006-1521-7
[32] Silva, R. F., & Zaniquelli, M. E. (2002). Morphology of nanometric size particulate aluminium-doped zinc oxide films. Colloids and Surfaces A: Physicochemical and Engineering Aspects, 198, 551-558. https://doi.org/10.1016/S0927-7757(01)00959-1
[33] Alkanad, K., Ali, O., GC, S. S., Hezam, A., Bajiri, M. A., & Lokanath, N. K. (2022, March). Highly Efficient Degradation of Organic Compounds via β-Bi2O3Semiconductor Under Visible Illumination. In IOP Conference Series: Materials Science and Engineering (Vol. 1221, No. 1, p. 012040). IOP Publishing. https://doi.org/10.1088/1757-899X/1221/1/012040
[34] Rahman, Q. I., Ahmad, M., Misra, S. K., & Lohani, M. (2013). Effective photocatalytic degradation of rhodamine B dye by ZnO nanoparticles. Materials Letters, 91, 170-174. https://doi.org/10.1016/j.matlet.2012.09.044
[35] Zada, N., Saeed, K., & Khan, I. (2020). Decolorization of Rhodamine B dye by using multiwalled carbon nanotubes/Co-Ti oxides nanocomposite and Co-Ti oxides as photocatalysts. Applied Water Science, 10(1), 1-10. https://doi.org/10.1007/s13201-019-1124-4
[36] Van Dao, D., Nguyen, T. T., Le, T. D., Kim, S. H., Yang, J. K., Lee, I. H., & Yu, Y. T. (2020). Plasmonically driven photocatalytic hydrogen evolution activity of a Pt-functionalized Au@ CeO 2 core-shell catalyst under visible light. Journal of materials chemistry A, 8(16), 7687-7694. https://doi.org/10.1039/D0TA00811G
[37] Khairnar, S. D., & Shrivastava, V. S. (2019). Facile synthesis of nickel oxide nanoparticles for the degradation of Methylene blue and Rhodamine B dye: a comparative study. Journal of Taibah University for Science, 13(1), 1108-1118. https://doi.org/10.1080/16583655.2019.1686248
[38] Wilhelm, P., & Stephan, D. (2007). Photodegradation of rhodamine B in aqueous solution via SiO2@ TiO2 nano-spheres. Journal of Photochemistry and Photobiology A: Chemistry, 185(1), 19-25. https://doi.org/10.1016/j.jphotochem.2006.05.003